Diabetology & Metabolic Syndrome

RESEARCH

Open Access

Electroacupuncture modulates the gut-brain axis via the PI3K/Akt pathway to improve feeding behavior, body weight, glucolipid metabolism, and reduce insulin resistance in T2DM rats

Shaoyang Liu[1†], Shuting Zhuang[1†], Rui Li[1*] and Haoru Duan[2]

Abstract

Background The rising prevalence and high mortality of diabetes have made it a significant public health concern. This study explores how electroacupuncture (EA) influences the PI3K/Akt pathway and its role in regulating the gut-brain axis, focusing on whether EA can modulate this axis via the PI3K/Akt pathway in the treatment of type 2 diabetes mellitus (T2DM). The research aims to reveal the mechanisms underlying EA's therapeutic effects and to investigate a novel strategy for managing T2DM.

Methods To induce T2DM in rat models, a high-fat diet and intraperitoneal injection of streptozotocin (STZ) were used. The rats were then randomly divided into four groups: a T2DM group, an EA group, an EA plus PI3K inhibitor group (EA + LY294002), and a control group (Con), which received a standard diet and a citric acid-sodium citrate solution. Following five weeks of intervention, assessments were conducted for food intake, body weight, fasting blood glucose (FBG), blood lipid profiles, and insulin resistance (IR). To analyze the PI3K/Akt pathway and gut-brain axis indices, various methods were employed, including Western blotting, qPCR, immunohistochemistry staining, HE staining, and 16 S rRNA sequencing.

Results Our research shows that EA improves food intake, body weight, FBG, lipid levels (TC, TG, HDL, LDL), serum insulin levels, IR and insulin sensitivity indices in T2DM rats. Additionally, EA boosts the expression of colonic tight junction proteins ZO-1, Occludin, and Claudin-1 while reducing intestinal inflammation and intestinal cell apoptosis. It also regulates Ghrelin and PYY levels in both colonic and hypothalamic tissues, improving the gut microbiota structure. These effects can be reversed by PI3K inhibitors.

†Shaoyang Liu and Shuting Zhuang contributed equally to this work and shared first authorship.

*Correspondence:
Rui Li
tingxuezhai@126.com

Full list of author information is available at the end of the article

Conclusions EA plays a role in managing feeding behavior, body weight, and glucolipid metabolism, as well as alleviating IR in T2DM rats. EA may contribute to the preservation of intestinal mucosal barrier integrity, likely through anti-inflammatory and anti-apoptotic actions mediated by the PI3K/Akt pathway. Additionally, EA appears to influence the regulation of brain-gut peptides and promote a healthier gut microbiota composition. These findings suggest that EA holds potential as an therapeutic approach for T2DM, with its mechanisms potentially linked to the modulation of the gut-brain axis via the PI3K/Akt pathway. Further research is warranted to fully elucidate these effects and their clinical implications.

Keywords Type 2diabetes mellitus, Electroacupuncture, PI3K/Akt pathway, Gut-brain axis

Introduction

Diabetes has swiftly become a major global health crisis. Its escalating prevalence, along with high mortality rates, poses significant threats to human health and places an immense burden on healthcare systems worldwide. Data from the Global Burden of Disease Study reveals that by 2021, an estimated 529 million people globally were diagnosed with diabetes. Of these cases, nearly 96% were attributed to type 2 diabetes mellitus (T2DM), establishing it as the most common form of the disease [1]. The impact of diabetes on mortality rates is profound, with the disease responsible for approximately 6.7 million deaths in 2021—equivalent to one life lost every five seconds. Beyond the human toll, diabetes imposes significant economic burdens on healthcare systems, with medical expenditures associated with diabetes reaching an estimated US$966 billion in 2021 [2]. These statistics highlight the urgent need for consistent and focused efforts to manage and prevent T2DM globally.

T2DM is mainly defined by a gradual decline in insulin production caused by pancreatic β-cell dysfunction. The precise mechanisms underlying T2DM remain incompletely understood, though two factors—β-cell dysfunction and insulin resistance (IR)—are consistently recognized as central to its progression [3, 4]. IR occurs when the body's tissues, especially muscle, liver, and adipose tissues, exhibit a diminished response to insulin signals, impeding glucose uptake and utilization. To counteract this resistance, the pancreas initially increases insulin production, often resulting in hyperinsulinemia. However, this compensation is not sustainable, and as IR progresses, β-cells become unable to meet the body's insulin demands. IR typically precedes the onset of T2DM, establishing it as a critical risk factor and a potential early marker for the disease [5, 6]. Excessive calorie intake and sedentary habits result in weight gain and metabolic stress, which raise the risk of insulin resistance and glucose intolerance. Interventions like weight loss, regular exercise, and balanced nutrition are highly effective for both prevention and management of T2DM and its complications [7–11]. Particularly, weight loss represents a key therapeutic strategy for improving insulin sensitivity, regulating glucolipid metabolism, and achieving sustainable T2DM management [12, 13]. Therefore, developing effective strategies for appetite regulation, weight management, and IR alleviation is essential for both T2DM prevention and treatment.

Acupuncture, a fundamental practice in traditional Chinese medicine, is extensively utilized in China as a therapeutic approach for T2DM and its complications. including peripheral neuropathy, nephropathy, and gastroparesis [14]. Research indicates that electroacupuncture (EA) effectively reduces IR, improves glucolipid metabolism, and decreases appetite and food intake, often with fewer gastrointestinal side effects compared to drug therapies [15–20]. Animal studies have also supported these findings to some extent [21–27]. However, the mechanisms behind acupuncture's effects remain unclear, limiting its broader use in T2DM treatment. Thus, further investigation into these mechanisms is essential for advancing its clinical application.

The gut-brain axis, a sophisticated communication network linking the gastrointestinal system and the central nervous system, has become a focal point in T2DM research. Enteroendocrine cells in the gut and the microbiota, a diverse community of microorganisms in the digestive tract, are crucial in facilitating the exchange of signals between the gut and the brain. This interaction profoundly impacts metabolism, immune function, and overall health [28]. Maintaining a healthy gut microbiota composition and strong intestinal mucosal barrier is essential for intestinal stability, while brain-gut peptides, secreted by enteric neuroendocrine cells, are vital for appetite regulation [29, 30]. In T2DM patients, gut microbiota disturbances typically involve reduced beneficial microbiota, increased opportunistic pathogens, and higher pro-inflammatory microbes [31–33]. Supplementing with probiotics may help address these imbalances [34, 35]. High-fat diets may weaken the integrity of the intestinal mucosal barrier, allowing pro-inflammatory substances to penetrate into the bloodstream. This permeability can trigger systemic inflammation, which may further exacerbate IR and other metabolic complications associated with T2DM [36, 37]. Repairing this barrier can reduce inflammation and improve IR [38, 39]. The gastrointestinal tract also secretes approximately 20 hormones, including Ghrelin, GLP-1, PYY, and CCK, which act on the hypothalamus, the brain's feeding center, to

regulate appetite. This complex interaction enables the gut to influence feeding behavior through the gut-brain axis [28, 40–44]. Disturbances in gut microbiota, weakened intestinal barriers, and imbalanced brain-gut peptide secretion can all disrupt energy intake, glucose and lipid metabolism, and IR. Therefore, maintaining a balanced gut-brain axis is essential for effective T2DM management.

The PI3K/Akt pathway is integral to several critical cellular processes, including glucose metabolism, IR, immune regulation, cell proliferation, and apoptosis [45–47]. PI3K is composed of enzymes that function within intracellular signaling pathways, while Akt—a serine/threonine kinase linked to protein kinase C—serves as its direct downstream target. When phosphorylated at all activation sites, Akt moves from the cell membrane to the cytoplasm or nucleus, transmitting signals to execute biological functions. Akt phosphorylation serves as a key indicator of PI3K activity, with downstream effectors Bcl-2 and Bax regulating apoptosis—Bcl-2 inhibiting it and Bax promoting it. Their heterodimer formation interferes with Caspase-mediated apoptotic signaling, supporting cell survival and growth [47, 48]. Within immune cells, especially macrophages, the PI3K/Akt pathway supports cell survival and encourages an anti-inflammatory response by reducing pro-inflammatory cytokine production and boosting anti-inflammatory cytokine levels. This anti-inflammatory action is crucial for mitigating chronic inflammation, a frequent condition associated with T2DM. Through its modulation of inflammatory responses, the PI3K/Akt pathway plays a key role in maintaining immune balance and promoting cellular health [48]. This pathway further contributes to maintaining the integrity of the intestinal mucosal barrier by regulating immune responses and controlling apoptosis in colonic cells [49, 50]. Disruption of this barrier can impair brain-gut peptide secretion by intestinal endocrine cells, which may alter hypothalamic control over food intake. Consequently, the PI3K/Akt signaling pathway could influence the gut-brain axis, potentially affecting central food intake regulation in T2DM by compromising mucosal barrier integrity.

Studies indicate that EA may assist in managing T2DM by modulating the PI3K/Akt signaling pathway. This modulation contributes to lowering FBG levels, reducing IR, and enhancing pancreatic β-cell function in T2DM rats [25, 50, 51]. Additionally, EA may affect the gut-brain axis within T2DM models, helping to restore the gut microbiota balance, boosting bile acid metabolism, reducing both intestinal and systemic inflammation, and strengthening intestinal barrier integrity. It also elevates GLP-1 levels in the hypothalamic nucleus, which helps regulate feeding behavior. Combined, these effects support improved glucolipid metabolism and further decrease IR [52–55].

EA may modulate both the PI3K/Akt signaling pathway and the gut-brain axis, however, the relationship between these mechanisms remains unclear. We hypothesize that the integrity of the intestinal mucosal barrier could serve as a link between them. This study investigates how EA influences the gut-brain axis in T2DM rats and whether it can modulate this axis through the PI3K/Akt pathway to facilitate the treatment of T2DM. Utilizing T2DM rat models, we examined the effects of EA on both the PI3K/Akt pathway and gut-brain axis, evaluating its potential to improve feeding behavior, body weight, glucolipid metabolism, and reduce IR. Our findings offer insights into the mechanisms by which EA may facilitate T2DM treatment, thereby supporting its prospective therapeutic application.

Materials and methods

Establishment of T2DM animal models, classification of groups and interventions

Twenty-four male SPF-grade Wistar rats, aged four weeks and weighing 150–180 g, were obtained from Sibeifu (Beijing) Biotechnology Co., Ltd. The rats were housed under standardized conditions, including a temperature of 23 ± 2 °C, humidity of 40 ± 5%, a 12-hour light/dark cycle, and free access to water. After a one-week acclimatization period, six rats were allocated to the control (Con) group, while the remaining 18 were designated for T2DM modeling. To induce T2DM, the 18 rats were fed a high-fat diet containing 10% lard, 20% sucrose, 2.5% cholesterol, and 0.5% sodium cholate for 4 weeks. Following a 16-hour fast, each rat received an intraperitoneal injection of 1% streptozotocin (STZ) solution at a dosage of 35 mg/kg. The STZ solution, prepared by dissolving STZ powder (Cat No. S0130, Lablead, Beijing, China) in 0.1 mol/L citrate-sodium citrate buffer, was kept on ice and shielded from light. T2DM was confirmed when FBG levels were ≥ 11.1 mmol/L on two occasions or random blood glucose (RBG) was ≥ 16.7 mmol/L [51, 56]. The 18 T2DM rats were then randomly divided into three groups of six: T2DM, EA, and EA with a PI3K inhibitor (EA + LY294002). The Con group continued on a standard diet, while the other groups remained on the high-fat diet throughout the intervention period.

Rats in the EA group were secured in custom-made cuffs, exposing the abdomen, back, and lower limbs, and allowed to acclimate for 5 min. Acupuncture was administered at four acupoints: Weiwanxiashu(EX-B3), Zhongwan(RN12), Zusanli(ST36), and Fenglong(ST40) bilaterally, using a 0.17*7 mm disposable sterile needle. Weiwanxiashu (EX-B3) is located 7 mm lateral to the depression under the 8th thoracic spinous process. Zhongwan (RN12) is located 20 mm above the umbilicus

on the midline of the upper abdomen. Zusanli (ST36) is located 5 mm inferior to the fibular head. Fenglong (ST40) is located on the middle of the fibula, about 7 mm below the fibular head [57–60]. The depths were 7 mm for EX-B3(oblique insertion) and 5 mm for RN12(oblique insertion), while ST36 and ST40 were needled directly to 7 mm. EA was applied by connecting ipsilateral EX-B3 and ST36 on alternating sides daily. The EA parameters were set to continuous waves at 15 Hz, with a current output of 1–3 mA. Needles were kept in place for 20 min with slight muscle twitching observed, avoiding any strong struggle from the rats. The treatments were carried out once a day, six days a week, over a period of five weeks. The EA + LY294002 group was administered intraperitoneal injections of the PI3K inhibitor once daily for a continuous period of 14 days (1.2 mg/kg in 0.5% CMC-Na solution; LY294002: Cat No.HY-10108, MedChemExpress, Shanghai, China; Cat No.CMC-Na: HY-Y0703, MedChemExpress, Shanghai, China) [61, 62], alongside the same EA protocol as the EA group. The Con and T2DM groups underwent the same handling and fixation procedures as the EA group, with unrestricted water access, once daily, 6 times per week, over a period of five weeks.

Sample collection

After the intervention, animals were fasted overnight without water. Fecal samples were collected sterilely. The rats were anesthetized via an intraperitoneal injection of 2% pentobarbital sodium at a dosage of 45 mg/kg. Blood samples (5–10 mL) were drawn from the abdominal aorta, centrifuged to separate the serum. After blood collection, hypothalamic and colonic tissues were excised and rinsed with 0.9% sodium chloride. A segment of the colonic tissue was fixed in 4% paraformaldehyde for morphological studies, while the remaining tissues were rapidly frozen in liquid nitrogen and stored at -80 °C to facilitate molecular analyses.

Assessment of basal index, glucolipid metabolism, and IR

Basal Index: (1)Weight: Body weights were recorded both prior to and following the intervention, after a 12-hour fasting period. (2)Food Intake: The remaining feed weight for each group was measured daily at a set time, with a predetermined amount of feed added simultaneously. Weekly average food intake for each group was then calculated. Glucolipid Metabolism Index: (1)FBG: FBG was measured with a Roche Accu-Chek blood glucose meter using tail blood samples from rats before modeling, before intervention, and after intervention, each following a 12-hour fast. (2)Blood Lipids: Serum levels of total cholesterol (TC), triglycerides (TG), low-density lipoprotein (LDL), and high-density lipoprotein (HDL) were quantified using an enzymatic colorimetric method. IR Index: (1)Serum Insulin Level: Measured via the ELISA method. (2)HOMA-IR and HOMA-ISI: Calculated as follows: HOMA-IR={Fasting serum insulin(mU/L)×Fasting glucose(mmol/L)}/22.5, and HOMA-ISI = 22.5/{Fasting serum insulin(mU/L)×Fasting glucose(mmol/L)}.

Western blotting(WB)

(1) Protein Extraction: 100 mg of colon and hypothalamic tissue was homogenized in a lysis solution, incubated on ice, and centrifuged (4 °C, 15 min, 10,000 rpm) to collect the supernatant. (2) Protein Quantification: The BCA assay measured protein content by comparing absorbance values at 562 nm against a BSA standard curve. (3)Protein Denaturation: Protein samples were mixed with loading buffer and RIPA solution (40 μg in 10 μL), and then heated (100 °C, 10 min) to denature the proteins. (4)Electrophoresis and Transfer: Protein samples (10 μL each) were loaded onto 10% separation and 5% stacking gels, run at 60 V until bromophenol blue reached the gel boundary, then at 200 V for 30 min. PVDF membranes were activated in ethanol before protein transfer at 400 mA for 30 min. (5)Blocking: The membranes were incubated in a 5% skim milk solution for 2 h at room temperature, and then washed with 1×TBST (10 min×3) to remove excess blocking agent and unbound proteins. (6)Primary Antibody Incubation: Primary antibodies were applied at 4 °C overnight, and then washed with 1×TBST (10 min×3). Antibody dilutions were as follows: PI3K(1:600), Akt(1:10000), Bcl-2(1:2500), Bax(1:10000), β-actin (1:5000), (Cat No. 60225-1-AP, 60203-2-Ig, 26593-1-AP, 60267-1-Ig, 66009-1-Ig, Proteintech Group, Chicago, USA); IL-6(1:1000), IL-10(1:1000), Occludin(1:500), Claudin-1(1:1000), Ghrelin(1:500), (Cat No. YP-Ab-16022, YP-Ab-15986, YP-Ab-07715, YP-Ab-16951, YP-Ab-15918, UpingBio, Hangzhou, China); ZO-1(1 μg/ml), PYY(1.9 μg/ml), (Cat No. PAC262Ra01, PAB067Ra01, Cloud-Clone Corp, Wuhan, China). (7)Secondary Antibody Incubation: The HRP-conjugated secondary antibodies were applied at room temperature for 1.5 h, and then washed with 1×TBST (10 min×3). Antibody dilutions were as follows: HRP-conjugated goat anti-mouse IgG(1:10000), HRP-conjugated goat anti-rabbit IgG(1:20000), (Cat No. SA00001-1, SA00001-2, Proteintech Group, Chicago, USA). (8)Detection and Analysis: The membranes were exposed using an ECL solution, and the optical density of each band was analyzed using ImageJ software (Version 1.8.0.112) for quantitative measurement. Target

protein expression levels were determined by the ratio of the target band's optical density to β-actin.

Quantitative PCR (qPCR)

(1) mRNA Extraction: Total mRNA was extracted from colon and hypothalamus tissues following the Total RNA Extraction Kit (Cat No.R1200, Solarbio, Beijing, China) protocol, then stored at -80 °C.
(2)Reverse Transcription: mRNA concentrations were recorded, and cDNA was obtained from the mRNA following the TOROBlue® All-in-One qRT Mix with dsDNase Kit (Cat No.RTQ-204, Toroivd, Shanghai, China) protocol, then stored at -20 °C.
(3)Fluorescence Quantification: PCR amplification was carried out using a Bio-Rad CFX Maestro 1.0 real-time cycler (ABI PRISM 7300, Applied Biosystems, Foster City, CA) under the following conditions: 95 10 min, (95 10s, 60 30s) 49 cycles, 65 5s, 95 0.5 C. The details of the specific primers utilized for qPCR analysis are presented in Table 1.
(4)Data Analysis: The relative expression levels of mRNA were determined through the $2^{\wedge-\Delta\Delta Ct}$ method, utilizing β-actin as the reference gene to ensure accurate normalization of the results.

Hematoxylin and Eosin (HE) staining

Histomorphological characteristics of rat colon tissue were analyzed through HE staining. Tissue samples embedded in paraffin were sliced into Sect. Conclusion μm thick, followed by heat drying at 65 °C. These sections underwent deparaffinization with xylene and were rehydrated stepwise using graded ethanol concentrations. Hematoxylin was applied for 3 min to stain the sections, after which they were rinsed thoroughly and inspected to ensure proper staining. A brief application of a differentiation solution was performed, and the reaction was halted by rinsing with tap water. Subsequently, the sections were counterstained with eosin for 1 min, and any residual stain was removed. Finally, the prepared slides were mounted using neutral gum and examined microscopically to assess the morphological details of the colon tissue.

Table 1 Primers for qPCR

Target genes	Primer pairs(5′ to 3′)	
	Forward	Reverse
PI3K	GCCGATCCTACAGTCCTATCCAATG	GCAGAAGGCACAGGTCCAGAG
Akt	AGGAGGAGGAGACGATGGACTTC	ACACGGTGCTTGGGCTTGG
Bcl-2	TGGAGAGCGTCAACAGGGAGATG	GGTGTGCAGATGCCGGTTCAG
Bax	GATGCGTCCACCAAGAAGCTGAG	CACGGCGGCAATCATCCTCTG
IL-6	ACTTCCAGCCAGTTGCCTTCTTG	TGGTCTGTTGTGGGTGGTATCCTC
IL-10	CTGCTCTTACTGGCTGGAGTGAAG	TGGGTCTGGCTGACTGGGAAG
ZO-1	GCCAAGCCAGTCCATTCTCAGAG	TCCATAGCATCAGTTTCGGGTTTCC
Occludin	CAACGGCAAAGTGAATGGCAAGAG	TCATCCACGGACAAGGTCAGAGG
Claudin-1	CTTCTGGGTTTCATCCTGGCTTCG	CCTGAGCAGTCACGATGTTGTCC
Ghrelin	ACCAGAAAGCCCAGCAGAGAAAG	CGAAGGGAGCATTGAACCTGATTTC
PYY	GGAGCTGAGCCGCTACTATGC	AGATTCTCGCTGTCGTCTGTGAAG
β-actin	ACCGTGAAAAGATGACCCAGCAT	CCAGAGGCATACAGGGACAA

Immunohistochemical (IHC) staining

Sections of paraffin-embedded rat colonic tissue, each cut to a thickness of 5 μm, underwent dewaxing followed by antigen retrieval in a citric acid solution heated for 15 min. To prevent non-specific antibody binding, the sections were treated with goat serum for 10 min and then incubated overnight at 4 °C with primary antibodies diluted as follows: ZO-1 (1:500), Occludin (1:500), and Claudin-1 (1:500). On the following day, the tissue sections were allowed to reach room temperature and rinsed thoroughly with PBS to remove unbound antibodies. Next, they were incubated in secondary antibodies, followed by tertiary antibodies, for 10 min each at room temperature to amplify the signal. Color development was achieved using a DAB chromogenic solution, which highlighted the target protein expression. The expression levels of tight junction proteins were visualized under a microscope. Images were captured for analysis, which was performed using ImageJ software to quantify and assess the protein expression levels accurately.

16 S rDNA amplicon sequencing

The rat intestinal microbiota was analyzed using the 16 S rDNA amplicon sequencing method. Methods: Genomic DNA was extracted from the samples using the OMEGA Soil DNA Kit (Cat No. D5625-01, Omega, Norcross, GA, USA). To target the microbial communities, the V3-V4 region of the 16 S rDNA gene was amplified by PCR, employing barcoded primers and high-fidelity DNA polymerase to ensure accurate amplification. Following amplification, the PCR products were verified using 2% agarose gel electrophoresis. The desired target fragments were then excised for further processing. DNA concentration was quantified with a BioTek FLx800 microplate reader to ensure precise measurements, and the samples were subsequently pooled in appropriate ratios for sequencing. Library construction was performed using the TruSeq Nano DNA LT Library Prep Kit (Illumina). The quality and integrity of the library were evaluated

using an Agilent Bioanalyzer 2100 and Promega QuantiFluor for quantification. Only samples that met the established quality standards were selected and sent for sequencing. Data Analysis: (1) Primary Data Processing: The raw sequencing data, initially in FASTQ format, were processed using Cutadapt to remove adapter sequences. The paired-end reads were then subjected to trimming, filtering for low-quality sequences, and denoising. The sequences were merged, and any chimeric sequences were eliminated using DADA2 within the QIIME2 platform. This processing resulted in the generation of representative reads and an amplicon sequence variant (ASV) abundance Table (2) Annotation: In QIIME2, the representative read for each ASV was selected for annotation. These reads were then compared to the Silva database (Version 138) using the classify-sklearn method for taxonomic classification. (3) Diversity Analysis: Microbial diversity within individual samples (α diversity) and differences in microbial community composition between samples (β diversity) were analyzed using QIIME2. This provided insights into the diversity, abundance and structure of microbial communities across the dataset.

Statistical methods

Statistical analyses were performed using SPSS software (version 27.0). Results from each group are expressed as the mean ± standard error of the mean (SEM). For datasets following a normal distribution and demonstrating homogeneity of variance, one-way ANOVA was employed, followed by the LSD post-hoc test to compare groups. When the data were normally distributed but violated the assumption of variance homogeneity, the Dunnett's T3 test was applied instead. A significance level of $P < 0.05$ was used to determine statistical significance.

Results

Effect of EA on body weight and food intake in rats

Figure 1A illustrates the body weight of rats across various groups following the modeling and intervention phases. After modeling, the T2DM, EA, and EA + LY294002 groups showed significantly higher body weights compared to the Con group. However, no notable differences were detected among the T2DM, EA, and EA + LY294002 groups. Following the intervention, the EA group experienced a significant decrease in body weight compared to the T2DM group. The EA + LY294002 group, however, exhibited a substantial increase in body weight compared to the EA group. Figure 1B highlights the changes in food intake among the groups after modeling and intervention. Post-modeling, food intake was notably higher in the T2DM, EA, and EA + LY294002 groups compared to the control group. After the intervention, food intake significantly decreased in the EA group, while it gradually increased in the EA + LY294002 group.

Effect of EA on glucolipid metabolism and IR in rats

Figure 1C illustrates the variations in FBG levels across the groups. Prior to modeling, no significant differences were observed in FBG levels among the groups. Following the modeling process, FBG levels in the T2DM, EA, and EA + LY294002 groups increased significantly compared to the Con group, confirming the successful establishment of the T2DM model. No notable differences in FBG levels were found among the T2DM, EA, and EA + LY294002 groups, allowing valid inter-group comparisons. After intervention, the T2DM group maintained significantly elevated FBG levels relative to the Con group. In contrast, the EA group exhibited a marked decrease in FBG compared to the T2DM group, while the EA + LY294002 group showed significantly higher FBG levels than the EA group. Figure 1D presents the serum levels of TG, TC, LDL, and HDL for each group. In the T2DM group, TG, TC, and LDL levels were significantly elevated, whereas HDL levels were notably reduced compared to the Con group. The EA group showed significant decreases in TG, TC, and LDL levels, along with an increase in HDL levels, compared to the T2DM group. Conversely, the EA + LY294002 group exhibited a significant rise in TG, TC, and LDL levels, as well as a decrease in HDL levels, relative to the EA group. Figure 1E illustrates the differences in INS levels, HOMA-IR, and HOMA-ISI among the groups. The T2DM group displayed significantly higher INS levels and HOMA-IR, accompanied by markedly lower HOMA-ISI, compared to the Con group. The EA group demonstrated a significant reduction in INS levels and HOMA-IR, alongside an increase in HOMA-ISI, relative to the T2DM group. In contrast, the EA + LY294002 group showed significantly elevated INS levels and HOMA-IR, with reduced HOMA-ISI compared to the EA group.

Effect of EA on the PI3K/Akt signaling pathway in the colon tissues of rats

Figure 2A, B highlight the protein and mRNA expression levels of PI3K, Akt, Bax, Bcl-2, IL-6, and IL-10 in rat colon tissues across various groups. In comparison to the Con group, the T2DM group demonstrated a significant reduction in the expression of PI3K, Akt, Bcl-2, and IL-10, coupled with a substantial increase in Bax and IL-6 levels. Following EA treatment, the levels of PI3K, Akt, Bcl-2, and IL-10 were significantly elevated compared to the T2DM group, while Bax and IL-6 levels were notably reduced. Conversely, in the EA + LY294002 group, the expression of PI3K, Akt, Bcl-2, and IL-10 was significantly downregulated, while Bax and IL-6 levels were markedly increased compared to the EA group.

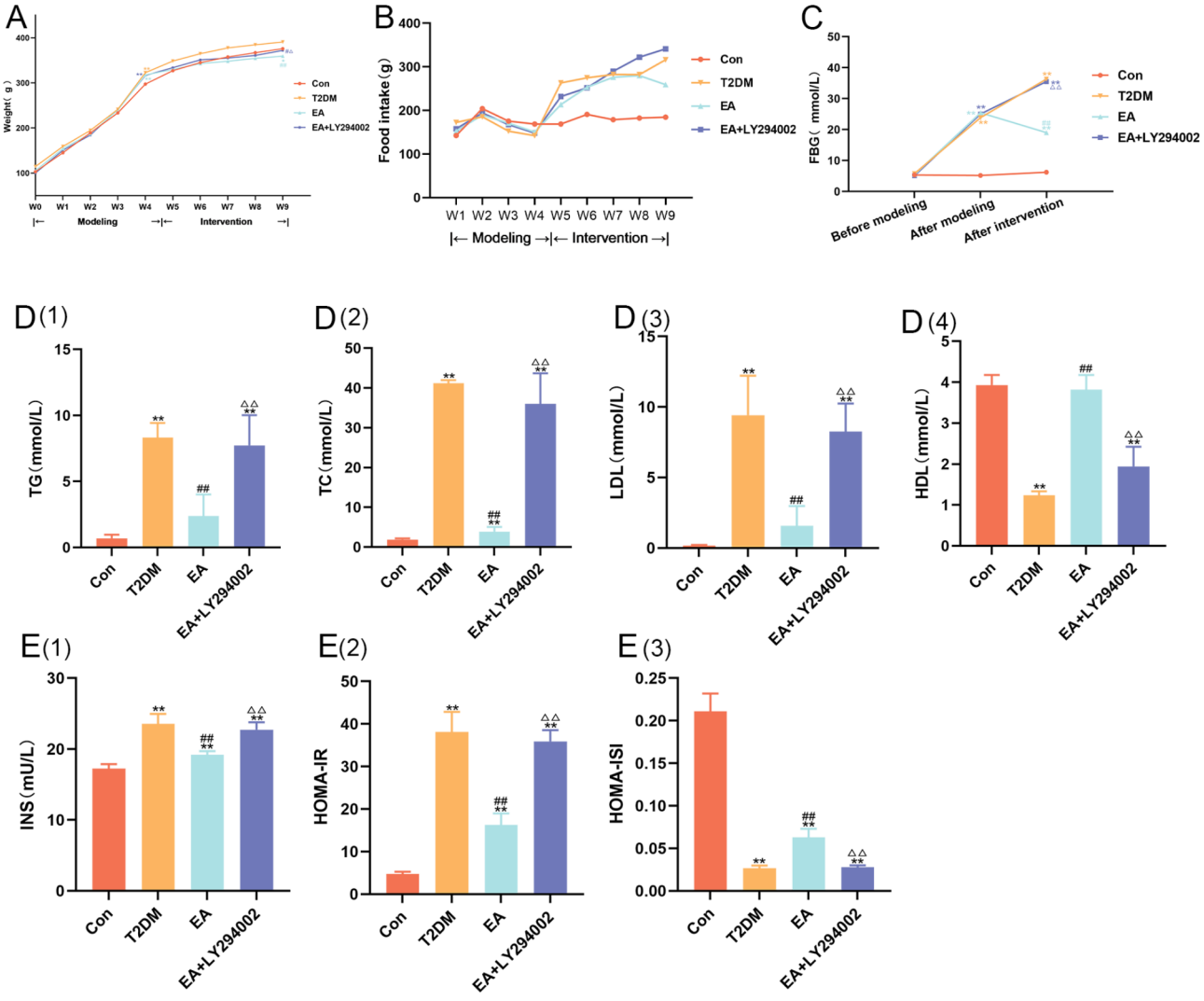

Fig. 1 Body weight, food intake, FBG, blood lipids, and IR in rats ($\bar{x} \pm \mathrm{SE}$, $n=6$). **A**: Weekly body weight for each group, in grams (g), with w1-4 representing modeling period and w5-9 intervention period; **B**: Weekly average food intake for each group, in grams (g), with w1-4 representing modeling period and w5-9 intervention period. **C**: FBG levels before modeling, after modeling and after intervention; **D**: Blood lipids, (1)TG, (2)TC, (3)LDL, (4)HDL. **E**: IR, (1) INS, (2)HOMA-IR, (3)HOMA-ISI. Con is the control group, T2DM is the model group, EA is the intervetion group, and EA + LY294002 is the intervention + PI3K inhibitor group. Compared to the Con group, $^{**}P<0.01$, $^{*}P<0.05$; compared to the T2DM group,$^{\#\#}P<0.01$, $^{\#}P<0.05$; compared to the EA group, $^{\triangle\triangle}P<0.01$, $^{\triangle}P<0.05$

Effect of EA on intestinal mucosal barrier in rats

Figure 3 illustrates the protein and mRNA expression levels of key intestinal mucosal barrier markers, including ZO-1, Occludin, and Claudin-1, in the colons of rats across different groups. In the T2DM group, the expression levels of ZO-1, Occludin, and Claudin-1 were significantly reduced compared to the Con group. However, the EA group exhibited a notable increase in the levels of these markers compared to the T2DM group. In contrast, the EA + LY294002 group demonstrated a significant reduction in ZO-1, Occludin, and Claudin-1 levels relative to the EA group.

Morphological changes of colon tissues in rats

Figure 4 highlights the morphological alterations observed in the colon tissues of rats across different experimental groups. In the Con group, the epithelial structure was intact with abundant goblet cells and no inflammation. In the T2DM group, epithelial integrity was compromised, with a significant reduction in goblet cells and extensive inflammation. The EA group showed clearer epithelial structures and more goblet cells than the T2DM group, though mild inflammation was present. In contrast, the EA + LY294002 group exhibited poor epithelial structure and persistent inflammation.

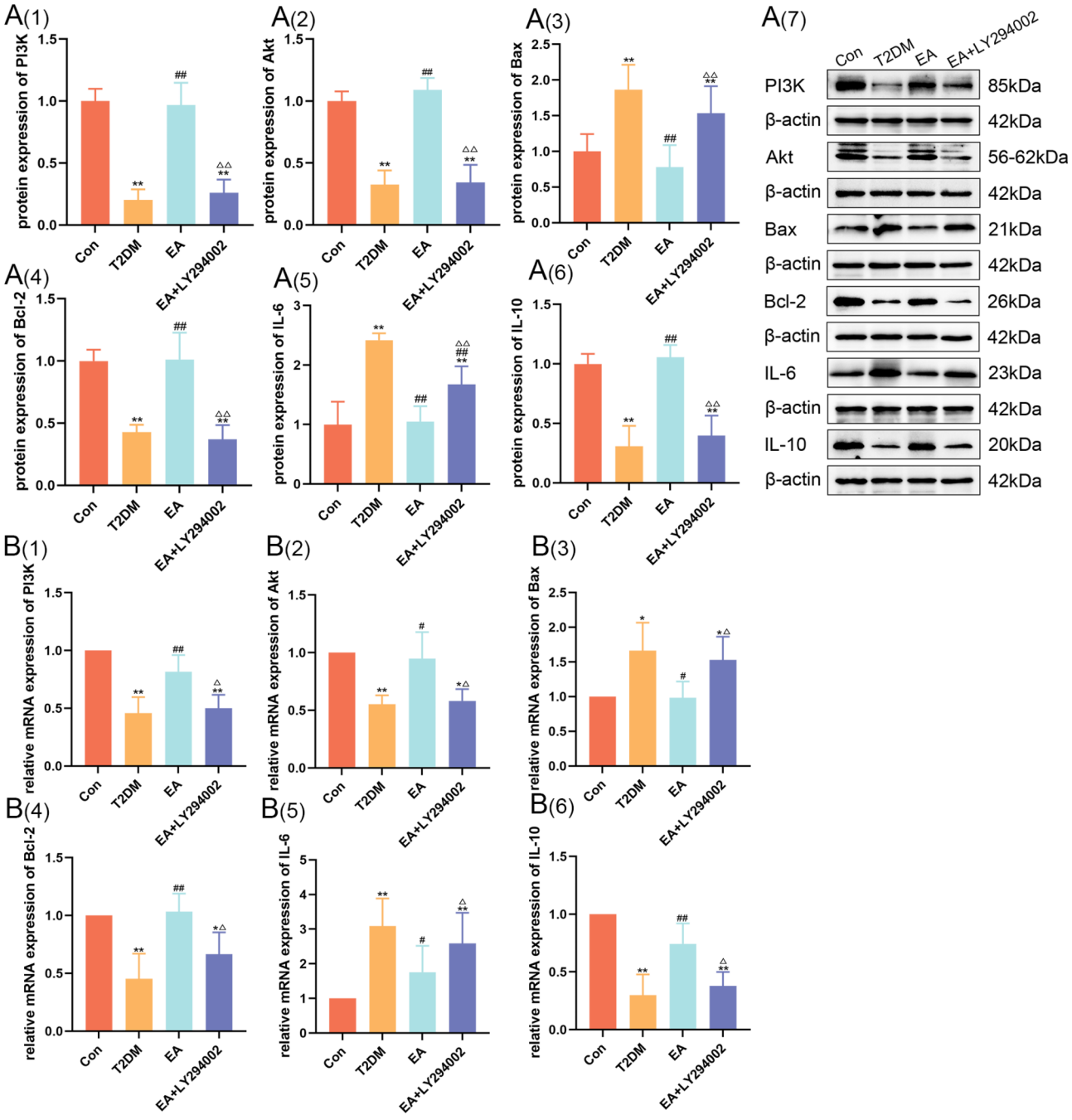

Fig. 2 Expression of the PI3K/Akt pathway in the colons of rats ($\bar{x} \pm \mathrm{SE}$, $n=6$). **A**: Protein expression levels related to the PI3K/Akt pathway, (1)-(6)quantifications for PI3K, Akt, Bax, Bcl-2, IL-6, and IL-10; (7) a diagram depicting protein expression bands. **B**: mRNA expression levels associated with the PI3K/Akt pathway, (1)-(6)quantifications for PI3K, Akt, Bax, Bcl-2, IL-6, and IL-10. Con is the control group, T2DM is the model group, EA is the intervetion group, and EA + LY294002 is the intervention + PI3K inhibitor group. Compared to the Con group, $^{**}P<0.01$, $^{*}P<0.05$; compared to the T2DM group,$^{\#\#}P<0.01$, $^{\#}P<0.05$; compared to the EA group, $^{\triangle\triangle}P<0.01$, $^{\triangle}P<0.05$

Effect of EA on Ghrelin and PYY in colon and hypothalamus in rats

Figure 5A displays the protein and mRNA expression levels of Ghrelin and PYY in the colonic tissues of rats across various experimental groups. In the T2DM group, Ghrelin expression was significantly elevated, while PYY expression was markedly reduced compared to the Con group. The EA group demonstrated a significant reduction in Ghrelin expression accompanied by a substantial increase in PYY levels relative to the T2DM group. However, in the EA + LY294002 group, Ghrelin levels were

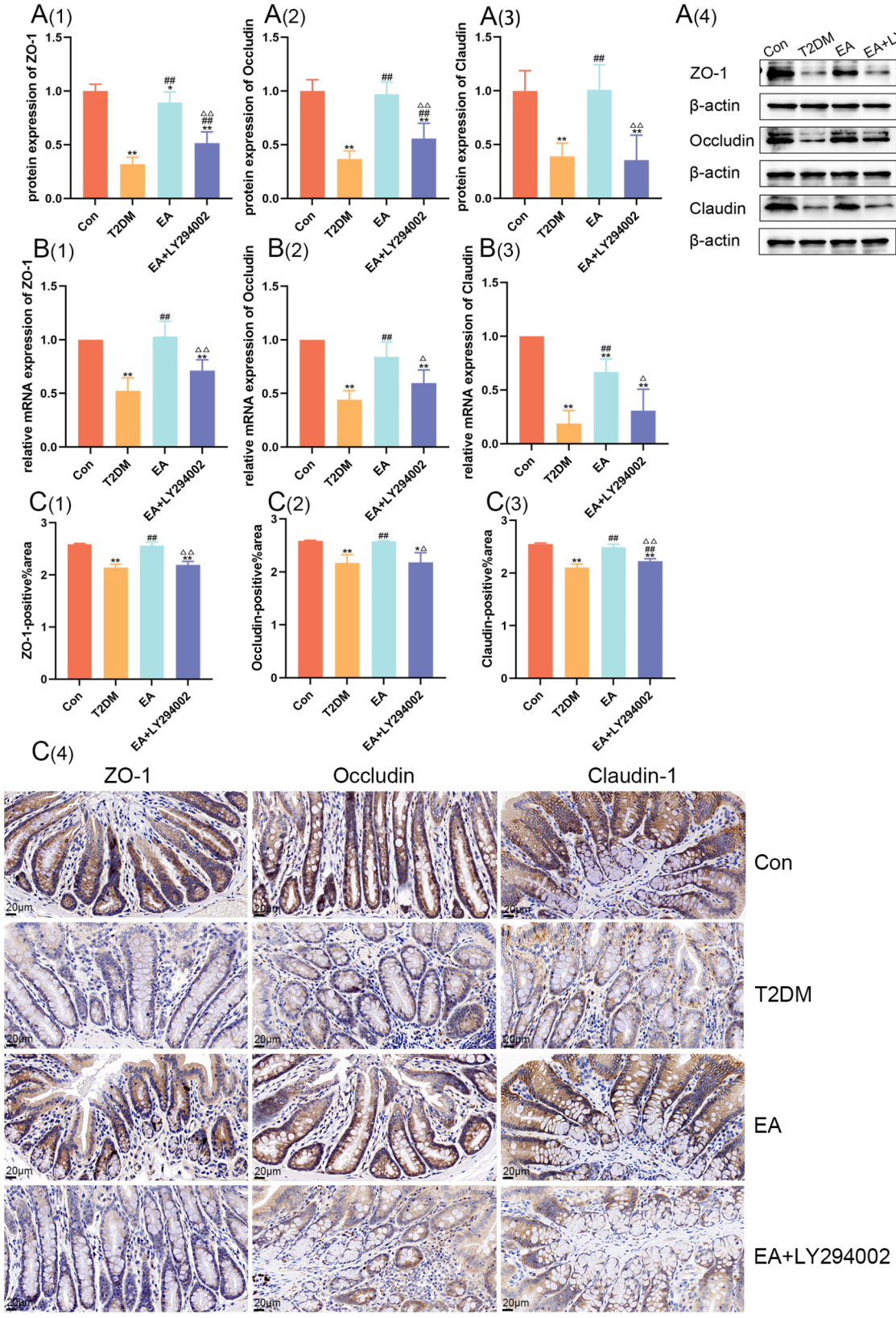

Fig. 3 (See legend on next page.)

(See figure on previous page.)

Fig. 3 Expression of ZO-1, Occludin and Claudin-1 in colon tissues of rats ($\bar{x} \pm SE$, $n=6$). **A**: Protein expression of ZO-1, Occludin, Claudin-1 in colon, (1) ZO-1, (2)Occludin, (3)Claudin-1, (4)a diagram depicting protein expression bands. **B**: The mRNA expression of ZO-1, Occludin, Claudin-1in colon, (1)ZO-1, (2)Occludin, (3)Claudin-1. C: Immunohistochemical staining of colon tissue of rats, (1)-(3)Quantitative analyses of ZO-1, Occludin and Claudin-1 based on immunohistochemical images according to groups; (4)Representative images of immunohistochemical staining of ZO-1, Occludin, Claudin-1 in colon, scale = 20 μm. Con is the control group, T2DM is the model group, EA is the intervention group, and EA + LY294002 is the intervention + PI3K inhibitor group. Compared to the Con group, $^{**}P<0.01$, $^{*}P<0.05$; compared to the T2DM group,$^{\#\#}P<0.01$, $^{\#}P<0.05$; compared to the EA group, $^{\triangle\triangle}P<0.01$, $^{\triangle}P<0.05$

significantly higher, and PYY levels were significantly lower compared to the EA group.

Figure 5B illustrates the protein expression levels of Ghrelin and both the protein and mRNA expression levels of PYY in the hypothalamic tissues of rats across groups. The expression patterns in the hypothalamus mirrored those observed in the colon. Compared to the Con group, the T2DM group exhibited significantly increased Ghrelin expression and decreased PYY expression. In the EA group, Ghrelin levels were significantly reduced, while PYY levels were significantly elevated compared to the T2DM group. Conversely, the EA + LY294002 group showed a significant increase in Ghrelin expression and a notable decrease in PYY levels compared to the EA group.

Effects of EA on diversity, abundance, structure and species distribution of gut microbiota in rats

The quality of the 16 S sequencing data was evaluated using the Rarefaction and Shannon curves, as shown in Fig. 6A. Both curves plateaued as sequencing depth increased, indicating sufficient coverage. This suggests that the number of strains identified in each sample reached saturation, capturing nearly all strain information. Figure 6B shows a Venn diagram based on ASV clustering and species annotation results. The Con group identified 3,310 ASVs, the T2DM group 936, the EA group 1,295, and the EA + LY294002 group 1,357. Compared to the Con group, the T2DM group had significantly fewer gut microbiota. However, the EA group showed an increase in gut microbiota following EA intervention.

The α-diversity index, which assesses the diversity and abundance of gut microbiota, includes key metrics such as the Shannon, Simpson, ACE, and Chao1 indices. As depicted in Fig. 6C, the T2DM group exhibited significantly lower Shannon, ACE, and Chao1 indices compared to the Con group, indicating reduced microbial diversity and abundance. Although the Simpson index also showed a decreasing trend, the change was not statistically significant. In the EA group, the Shannon index was significantly elevated compared to the T2DM group, suggesting a partial restoration of gut microbiota diversity. However, the other indices showed an upward trend without reaching statistical significance. Notably, no significant differences were observed between the EA + LY294002 group and the EA group across any of the indices.

The β-diversity analysis compares the structural similarities and differences in gut microbiota. In this study, the β diversity index, Principal Coordinates Analysis (PCoA) and Non-Metric Multi-Dimensional Scaling (NMDS) analysis were employed for evaluation. Intergroup comparisons of the β-diversity index, based on Weighted Unifrac and Bray-Curtis distances, are shown in Fig. 6D (1)(2). The T2DM group exhibited a significant decrease in β-diversity compared to the Con group. In contrast, the EA group showed a significant increase in β-diversity compared to the T2DM group. However, the β-diversity index in the EA + LY294002 group was significantly lower than in the EA group. In PCoA and NMDS, smaller sample distances indicate greater similarity in species composition. The PCoA results based on Weighted Unifrac and Bray-Curtis distances are shown in Fig. 6D (3)(4), and the NMDS results using Unifrac and Bray-Curtis distances are in Fig. 6D (5)(6). Both analyses revealed similar trends: the T2DM and Con groups showed the largest distance with no overlap. Distances between groups, in descending order, were: Con vs. T2DM, Con vs. EA + LY294002, and Con vs. EA.

The top ten most abundant genera in each group were selected, and a species classification tree analysis was performed on the gut microbiota of rats. Figure 6E shows two key bacterial families related to our study: Muribaculaceae and Akkermansia. The relative abundance of Muribaculaceae was lower in the T2DM group compared to the Con group, higher in the EA group than in T2DM, and reduced in the EA + LY294002 group compared to the EA group. Conversely, Akkermansia was less abundant in the Con group, but more abundant in the T2DM, EA, and EA + LY294002 groups, with the following ranking: EA > EA + LY294002 > T2DM.

Discussion

IR is a key mechanism in the pathogenesis of T2DM. Obesity, driven by poor dietary habits, significantly contributes to T2DM development. Animal studies show that acupuncture regulates appetite and body weight by stimulating the hypothalamic feeding center, including the activation or inhibition of nuclei like ARC, VMH, and LHA [26, 63]. Both clinical and animal research confirm that EA improves glucolipid metabolism and reduces IR in T2DM [15–20]. Food intake serves as an indicator of

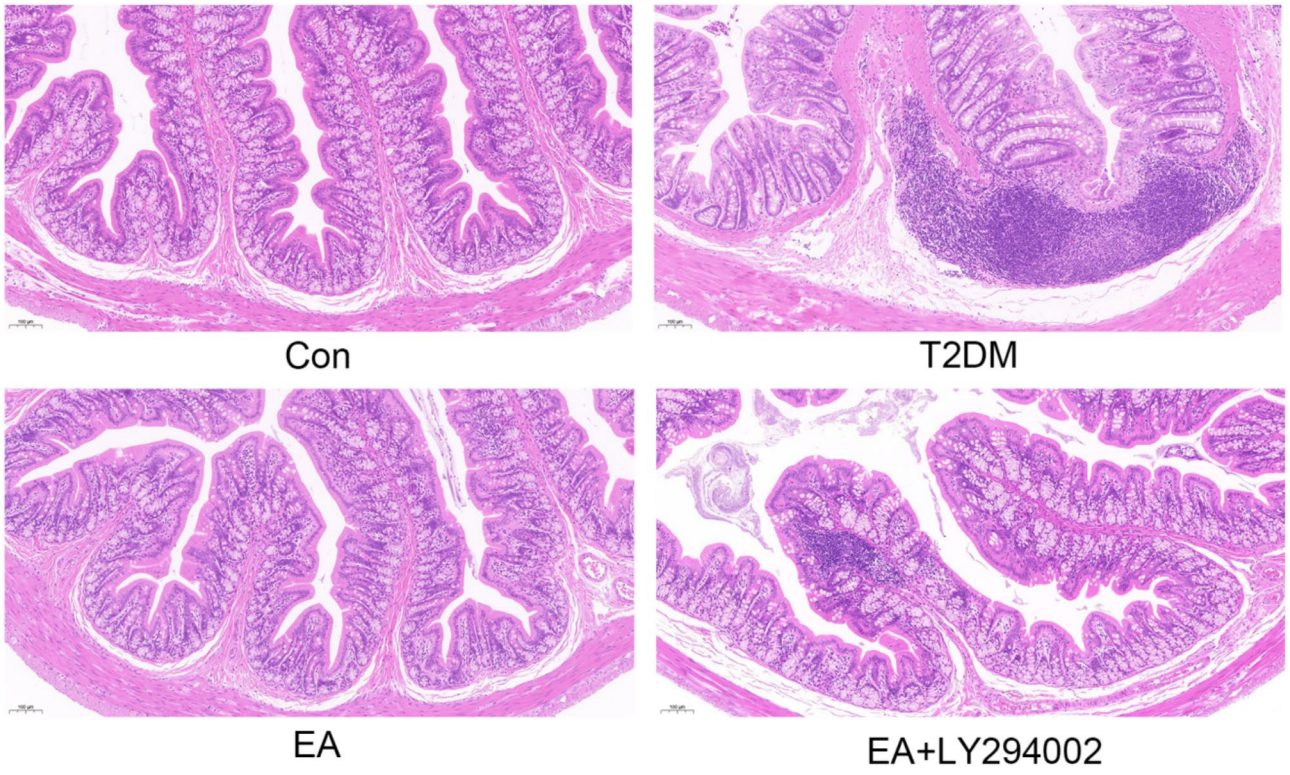

Fig. 4 HE staining of colon tissue of rats in each group (100X), scale = 100 μm. Con is the control group, T2DM is the model group, EA is the intervention group, and EA + LY294002 is the intervention + PI3K inhibitor group

feeding behavior and gastrointestinal function in rats. In this study, following the T2DM modeling, food intake in the T2DM, EA, and EA + LY294002 groups significantly increased compared to the Con group, reflecting the polyphagia characteristic of T2DM. After 5 weeks of EA treatment, food intake in the EA group declined compared to the T2DM group, with a marked reduction observed toward the end of the intervention, suggesting that EA inhibits feeding behavior in these rats. T2DM rats also exhibited greater weight gain post-modeling, with an accelerated increase in body weight compared to the Con group. However, EA treatment effectively reduced the weight gain in T2DM rats. After the 5-week intervention, EA significantly lowered FBG, serum TG, TC, and LDL levels, while increasing HDL levels. Such changes indicate an enhanced lipid and glucose metabolism in T2DM rats treated with EA. Additionally, the observed decrease in serum insulin and HOMA-IR values, coupled with an increase in HOMA-ISI, further supports the notion that EA enhances insulin sensitivity, potentially mitigating IR-a key characteristic of T2DM. The reversal of these benefits by the PI3K inhibitor LY294002 underscores the critical role of the PI3K/Akt signaling pathway in mediating EA's effects in regulating feeding behavior, reducing body weight, improving glucolipid metabolism, and enhancing insulin sensitivity.

The intestinal mucosal barrier is a complex structure composed of multiple defense systems, including mechanical, microbial, chemical, and immune elements. This barrier is essential for maintaining physiological homeostasis by creating a selective yet protective interface between the external environment within the gut and the internal environment of surrounding tissues and organs. The mechanical barrier specifically includes the mucosal layer, intestinal epithelial cells, tight junctions, and the submucosal propria, all of which work together to form a physical shield against harmful substances. Of particular importance are the tight junction proteins-Occludin, Claudin, and ZO-which function as gatekeepers, preventing the translocation of pathogens and toxins across the intestinal lining. These tight junctions tightly regulate permeability, thereby minimizing bacterial invasion and preserving mucosal integrity, which is critical for preventing systemic infection and inflammation [64]. The PI3K/Akt signaling pathway is central to maintaining the stability and integrity of the intestinal mucosal barrier. By modulating cell proliferation, apoptosis or inflamation, PI3K/Akt signaling contributes significantly to tissue repair and cellular resilience under various stress conditions. Researches have demonstrated that compounds derived from traditional Chinese medicine can activate the PI3K/Akt pathway, effectively reducing apoptosis and reinforcing the intestinal barrier against potential

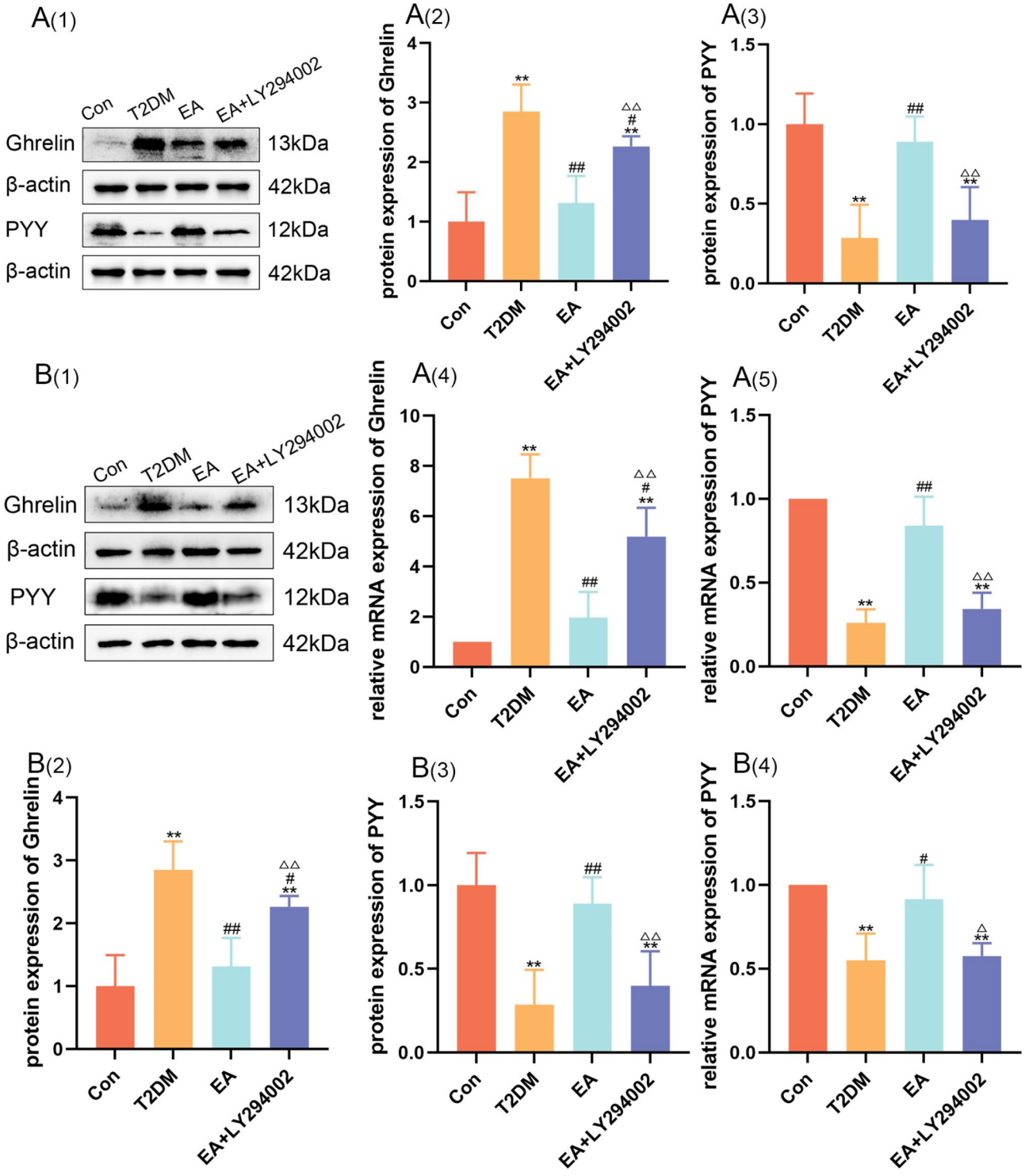

Fig. 5 Expression of Ghrelin and PYY in colon and hypothalamus of rats($\bar{x} \pm \mathrm{SE}$, $n=6$). **A**: Expression of Ghrelin and PYY in the colon, (1)a diagram depicting protein expression bands, (2)(3)protein expression levels of Ghrelin and PYY, (4)(5)mRNA expression levels of Ghrelin and PYY; **B**: Expression of Ghrelin and PYY in the hypothalamus, (1)a diagram depicting protein expression bands, (2)(3)protein expression levels of Ghrelin and PYY, (4)mRNA expression level of PYY. Con is the control group, T2DM is the model group, EA is the intervention group, and EA + LY294002 is the intervention + PI3K inhibitor group. Compared to the Con group, $^{**}P<0.01$, $^{*}P<0.05$; compared to the T2DM group,$^{\#\#}P<0.01$, $^{\#}P<0.05$; compared to the EA group, $^{\triangle\triangle}P<0.01$, $^{\triangle}P<0.05$

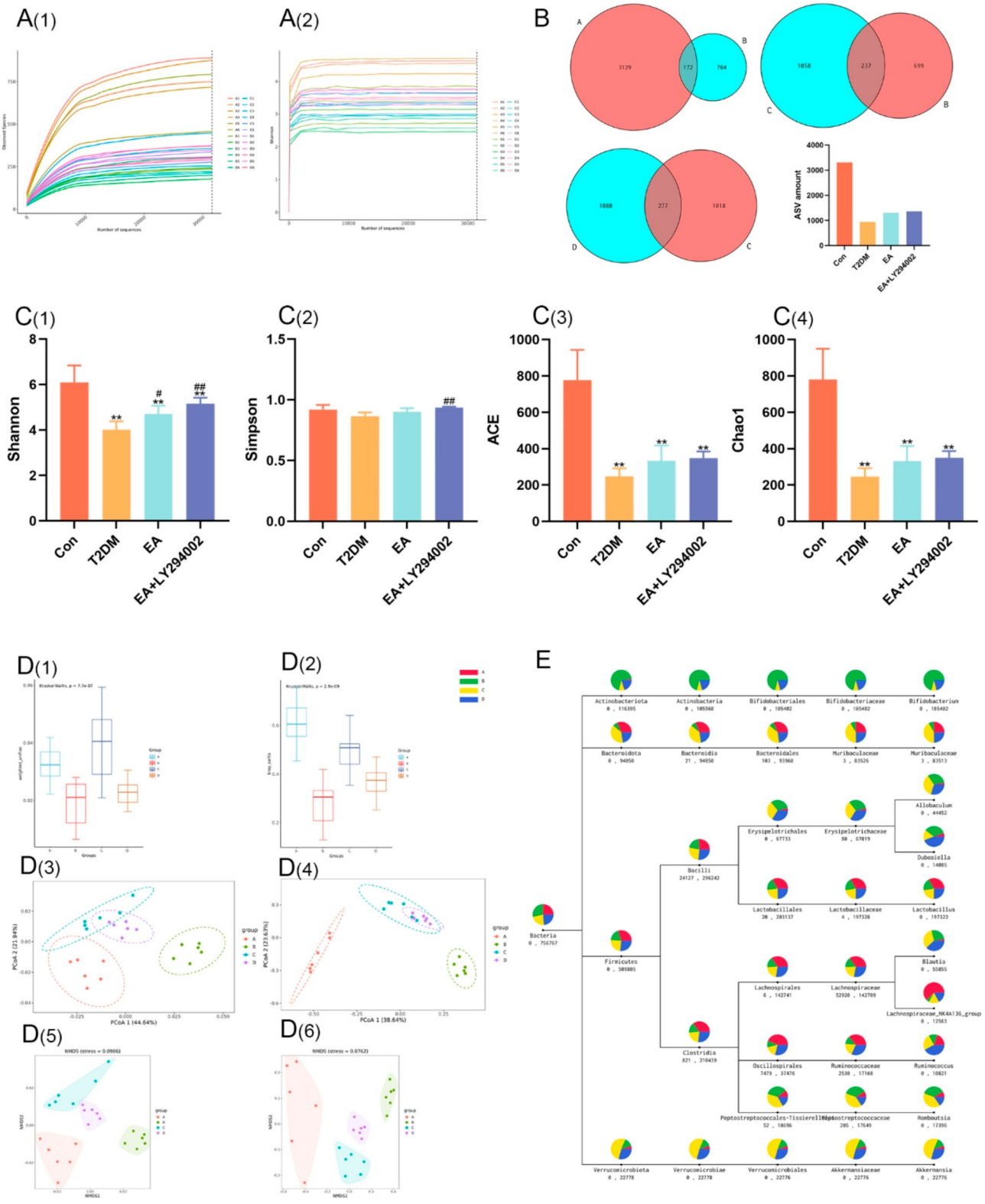

Fig. 6 (See legend on next page.)

(See figure on previous page.)

Fig. 6 Diversity, abundance, structure, species distribution of gut microbiota of rats($\bar{x} \pm SE$, $n=6$). **A**: Quality assessment of sequencing data. (1)Rarefaction curve, (2)Shannon curve, The abscissa represents the amount of randomly selected sequencing data and the ordinate indicates the number of observed ASVs. **B**: Venn diagram based on ASV clustering and species annotation results, with the number inside the circle indicating the count of ASVs and the number outside denoting the corresponding group. **C**: The α diversity index. (1)Shannon, (2)Simpson, (3)ACE, (4)Chao1. **D**: The β diversity analysis. (1)(2)β-diversity based on Weighted Unifrac distance and Bray Curtis distance. (3)(4)PCoA analysis based on Weighted Unifrac distance and Bray-Curtis distance. The abscissa and ordinate represent two principal components, with the percentage indicating each component's contribution to sample variation. Points correspond to samples, grouped by color. (5)(6)NMDS analysis based on Weighted Unifrac distance and Bray-Curtis distance. Each point represents a sample, with the distance between points indicating sample differences. Identical colors denote samples from the same group. Stress < 0.2 indicates accurate representation of sample differences. **E**: The species-specific classification tree of the gut microbiota in rats in each group. The colors in the circles represent different groups (see legend), while the fan size reflects the relative abundance ratio. The first number below each circle shows the count of uniquely aligned sequences, and the second number represents the total number of aligned sequences. A/Con is the control group, B/T2DM is the model group, C/EA is the intervention group, and D/EA + LY294002 is the intervention + PI3K inhibitor group. Compared to the Con group, $^{**}P<0.01$; compared to the T2DM group, $^{\#\#}P<0.01$, $^{\#}P<0.05$

damage [50, 65–67]. Similarly, liraglutide, a GLP-1 receptor agonist, has shown protective effects on the intestinal mucosa, particularly under conditions of ischemia-reperfusion injury. Liraglutide achieves this by promoting PI3K/Akt phosphorylation, which reduces inflammation and prevents apoptosis within the mucosal lining [68]. Collectively, these findings emphasize the essential role of the PI3K/Akt signaling pathway in sustaining intestinal mucosal barrier integrity. This study examined the regulatory effects of EA on the PI3K/Akt signaling pathway within the colonic tissue of T2DM rats. Following T2DM modeling, the rats exhibited suppressed PI3K/Akt signaling, leading to an increase in Bax (a pro-apoptotic protein) and a decrease in Bcl-2 (an anti-apoptotic protein). This imbalance was accompanied by heightened levels of IL-6 (a pro-inflammatory cytokine) and reduced levels of IL-10 (an anti-inflammatory cytokine), indicating aggravated apoptosis and inflammation in intestinal cells. EA treatment effectively reactivated the PI3K/Akt pathway in the colonic tissue, resulting in a decrease in Bax and IL-6 levels while enhancing Bcl-2 and IL-10 expression. These changes suggest that EA mitigates both apoptosis and inflammation in the intestinal cells of T2DM rats. However, when PI3K inhibitors were applied, these beneficial effects of EA were reversed, confirming that EA's Anti-apoptosis and anti-inflammatory impact on colonic tissue operates primarily through the activation of the PI3K/Akt signaling pathway.

Studies have demonstrated that acupuncture can protect the intestinal mucosal barrier in various animal models, especially in conditions such as irritable bowel syndrome, ulcerative colitis, Alzheimer's disease, Parkinson's disease, acute pancreatitis, and uremia. However, despite this growing evidence, there is still limited research on the specific effects of acupuncture on the intestinal mucosal barrier in the context of T2DM, leaving an important area for future exploration [69–75]. The anti-apoptotic and anti-inflammatory effects mediated by the PI3K/Akt pathway may play a crucial role in preserving the integrity of the intestinal barrier in T2DM rats. By maintaining this barrier, PI3K/Akt signaling supports the optimal function of the gut-brain axis, which is essential for overall metabolic and immune stability. Our findings indicate that EA significantly improves intestinal health in T2DM rats by enhancing mucosal barrier integrity and reducing inflammation, which may contribute to better overall metabolic outcomes. In T2DM rats, we observed marked reductions in the expression of key mucosal barrier proteins, including ZO-1, Occludin, and Claudin-1, accompanied by notable infiltration of inflammatory cells within the colonic tissue. These changes suggest a compromised intestinal barrier and heightened inflammatory response. By restoring the expression of ZO-1, Occludin, and Claudin-1, EA strengthens the intestinal barrier, potentially preventing the translocation of harmful bacteria and toxins that could exacerbate metabolic dysfunction. Additionally, the reduction in inflammatory cell infiltration observed in EA-treated rats indicates a dampening of local intestinal inflammation, which is crucial for maintaining mucosal homeostasis. Notably, the beneficial effects of EA on both barrier protein expression and inflammation were reversed when PI3K inhibitors were administered, suggesting that the PI3K/Akt signaling pathway plays a pivotal role in mediating EA's protective effects in the integrity of the intestinal barrier.

Brain-gut peptides and gut microbiota are essential components that influence the gut-brain axis. In this study, we examined alterations in the gut-brain axis of T2DM rats, focusing on the roles of brain-gut peptides and gut microbiota. Additionally, we assessed how EA modulates these components. Our study highlights the role of EA in modulating key food intake-related brain-gut peptides, specifically Ghrelin and PYY, to improve feeding behavior in T2DM rats through the PI3K/Akt signaling pathway. Ghrelin, an appetite-stimulating hormone primarily produced by X-like cells in the stomach, acts on the hypothalamus to increase food intake, while Peptide YY (PYY), synthesized by intestinal L cells, suppresses appetite and delays gastric emptying [28, 40, 43]. In T2DM rats, we observed an imbalance in these peptides, with increased Ghrelin and decreased PYY levels in both the colon and hypothalamus, indicating a disrupted appetite regulation mechanism likely contributing to hyperphagia in diabetes. EA treatment corrected this

imbalance by reducing Ghrelin levels and raising PYY levels, suggesting a normalization of appetite signals and a potential mechanism by which EA reduces food intake in T2DM rats. Notably, the beneficial effects of EA on these peptides were reversed when PI3K inhibitors were applied, supporting the hypothesis that EA's modulation of Ghrelin and PYY is mediated via the PI3K/Akt signaling pathway. By targeting the PI3K/Akt pathway to balance appetite-regulating peptides, EA may offer a novel approach to managing feeding behavior in T2DM. These findings lay a foundation for further research into the potential of EA as a therapeutic intervention in T2DM by modulating gut-brain axis components.

We analyzed the gut microbiota structure and species distribution in T2DM rats through ASV clustering and species annotation. To evaluate microbial diversity and abundance, we applied the α-diversity indices, specifically the Shannon and Simpson indices for diversity, and the ACE and Chao1 indices for abundance. All four metrics were positively correlated, ensuring a robust and multifaceted assessment of gut microbial diversity. Additionally, we conducted β-diversity analysis to examine the variations in microbial community structure across different samples. By employing β-diversity indices along with PCoA and NMDS, we were able to identify both similarities and differences in the gut microbiota communities [76–78]. Our findings reveal that EA has a restorative impact on gut microbiota in T2DM rats, suggesting its potential in modulating the gut-brain axis to treat T2DM. T2DM modeling led to a decrease in overall gut microbiota numbers, diversity, and abundance, along with significant alterations in the microbial community structure. This dysbiosis is commonly associated with metabolic disorders, as disruptions in gut microbial balance can exacerbate inflammation, IR, and metabolic imbalance. EA intervention effectively countered these negative effects, restoring microbiota numbers, enhancing diversity and abundance, and reversing structural changes induced by T2DM. Previous studies have suggested that EA affects gut microbiota by altering the abundance of Firmicutes and Bacteroides and shifting the Firmicutes/Bacteroides ratio [79, 80]. Notably, our study found that PI3K inhibitors reversed the improvements EA conferred on β-diversity, which reflects the structural composition of the gut microbiota, while α-diversity—indicative of overall diversity and abundance—remained unaffected by the inhibitors. This suggests that EA's effects on microbiota structure may involve the PI3K/Akt signaling pathway, while its influence on diversity and abundance is likely independent of this pathway.

Subsequently, we analyzed the species distribution of gut microbiota across all groups by selecting the top ten genera with the highest abundance for species classification tree analysis in T2DM rats [81]. Muribaculaceae, known for producing short-chain fatty acids, supports host health by strengthening the intestinal barrier and regulating immune responses. Reasearch shows that its increase is linked to the efficacy of hypoglycemic agents [82]. In T2DM rats, the abundance of Muribaculaceae was significantly reduced, likely contributing to compromised gut health and metabolic imbalance. EA intervention effectively increased Muribaculaceae levels, a change that was reversed upon administration of PI3K inhibitors, indicating that EA's impact on Muribaculaceae may be mediated through the PI3K/Akt signaling pathway. Similarly, Akkermansia, a genus primarily located in the intestinal mucus layer, plays a vital role in barrier function, mucus production, and metabolic and immune regulation [83]. We found Akkermansia abundance to be highest in the EA group, followed by the EA + LY294002 and T2DM groups, suggesting that EA enhances Akkermansia levels, which may reinforce gut barrier integrity and support immune balance. The varying effects observed with and without PI3K inhibitors suggest that the PI3K/Akt pathway may contributes to EA's influence on these microbial populations. These findings underscore EA's potential to modulate beneficial gut microbiota and highlight the PI3K/Akt pathway as a key mediator in enhancing gut health in T2DM rats.

Conclusion

In this study, STZ-induced T2DM rats were utilized as research subjects, with the PI3K/Akt pathway and gut-brain axis serving as entry points. Various methods, including WB, qPCR, IHC staining, HE staining, and 16 S rRNA sequencing, were employed to investigate the mechanisms underlying EA intervention in T2DM rats. The results showed that EA regulates feeding behavior, body weight, glucolipid metabolism, and alleviates IR. It may contribute to the preservation of intestinal mucosal barrier integrity, likely through anti-apoptotic and anti-inflammatory effects mediated by the PI3K/Akt pathway. Additionally, EA appears to influence the regulation of brain-gut peptides related to food intake and promote a more balanced gut microbiota composition. In conclusion, EA may serve as treatment for T2DM, with its mechanisms potentially linked to the regulation of the gut-brain axis via the PI3K/Akt pathway. However, this study has limitations that should be acknowledged, and further research is warranted to fully elucidate these effects and their clinical implications. Specifically, the precise mechanisms governing the interactions among various components of the gut-brain axis during EA therapy for T2DM remain to be fully elucidated. Furthermore, large-scale clinical trials are needed to confirm EA's efficacy and safety in human patients. This study focused on EA as a standalone intervention; future studies should investigate its potential synergistic

effects when combined with pharmacological therapies, which may enhance therapeutic outcomes while reducing adverse effects.

Acknowledgements
The authors thank the School of Acupuncture-Moxibustion and Tuina, Beijing University of Chinese Medicine for supplied experimental equipment and research environment.

Author contributions
SL: Project management, data analysis, and manuscript writing. SZ: Indicator detection and methodological support. RL: Design guidance, supervision, and funding acquisition. HD: Data proofreading and visualization. All authors read and approved the final manuscript.

Funding
This study was supported by the following grants: (1) National Natural Science Foundation of China (Grant Nos. 82474652); (2) Beijing Municipal Natural Science Foundation (Grant Nos. 7232276).

Data availability
No datasets were generated or analysed during the current study.

Declarations

Ethical approval
The protocol received approval from the Laboratory Animal Welfare and Ethics Committee of Beijing University of Chinese Medicine (BUCM-202305001-2076).

Competing interests
The authors declare no competing interests.

Author details
[1]School of Acupuncture-Moxibustion and Tuina, Beijing University of Chinese Medicine, Beijing 100029, China
[2]Department of Acupuncture and Moxibustion, Chaoyang District Traditional Chinese Medicine Hospital, Beijing 100026, China

Received: 16 November 2024 / Accepted: 30 March 2025
Published online: 09 April 2025

References

1. GBD 2021 Diabetes Collaborators. Global, regional, and National burden of diabetes from 1990 to 2021, with projections of prevalence to 2050: a systematic analysis for the global burden of disease study 2021. Lancet. 2023;402(10397):203–34.
2. Magliano DJ, Boyko EJ. IDF diabetes atlas 10th edition scientific committee. IDF DIABETES ATLAS. 10th ed. Brussels: International Diabetes Federation; 2021.
3. Roden M, Shulman GI. The integrative biology of type 2 diabetes. Nature. 2019;576(7785):51–60.
4. Kahn SE, Hull RL, Utzschneider KM. Mechanisms linking obesity to insulin resistance and type 2 diabetes. Nature. 2006;444(7121):840–6.
5. Saltiel AR, Kahn CR. Insulin signalling and the regulation of glucose and lipid metabolism. Nature. 2001;414(6865):799–806.
6. Lu X, Xie Q, Pan X, et al. Type 2 diabetes mellitus in adults: pathogenesis, prevention and therapy. Signal Transduct Target Ther. 2024;9(1):262.
7. Tinajero MG, Malik VS. An update on the epidemiology of type 2 diabetes: A global perspective. Endocrinol Metab Clin North Am. 2021;50(3):337–55.
8. Zheng Y, Ley SH, Hu FB. Global aetiology and epidemiology of type 2 diabetes mellitus and its complications. Nat Rev Endocrinol. 2018;14(2):88–98.
9. Diabetes Prevention Program Research Group. Long-term effects of lifestyle intervention or Metformin on diabetes development and microvascular complications over 15-year follow-up: the diabetes prevention program outcomes study. Lancet Diabetes Endocrinol. 2015;3(11):866–75.
10. Diabetes Prevention Program Research Group, Knowler WC, Fowler SE, et al. 10-year follow-up of diabetes incidence and weight loss in the diabetes prevention program outcomes study. Lancet. 2009;374(9702):1677–86.
11. Lindström J, Louheranta A, Mannelin M, et al. The Finnish diabetes prevention study (DPS): lifestyle intervention and 3-year results on diet and physical activity. Diabetes Care. 2003;26(12):3230–6.
12. Szczerba E, Barbaresko J, Schiemann T, Stahl-Pehe A, Schwingshackl L, Schlesinger S. Diet in the management of type 2 diabetes: umbrella review of systematic reviews with meta-analyses of randomised controlled trials. BMJ Med. 2023;2(1):e000664.
13. Dambha-Miller H, Day AJ, Strelitz J, Irving G, Griffin SJ. Behaviour change, weight loss and remission of type 2 diabetes: a community-based prospective cohort study. Diabet Med. 2020;37(4):681–8.
14. Feng Y, Fang Y, Wang Y, Hao Y. Acupoint therapy on diabetes mellitus and its common chronic complications: A review of its mechanisms. Biomed Res Int. 2018;2018:3128378.
15. Wen Q, Hu M, Lai M, et al. Effect of acupuncture and Metformin on insulin sensitivity in women with polycystic ovary syndrome and insulin resistance: a three-armed randomized controlled trial. Hum Reprod. 2022;37(3):542–52.
16. Mooventhan A, Ningombam R, Nivethitha L. Effect of bilateral needling at an acupuncture point, ST-36 (Zusanli) on blood glucose levels in type 2 diabetes mellitus patients: A pilot randomized placebo controlled trial. J Complement Integr Med. 2020;17(3). https://doi.org/10.1515/jcim-2019-0100. Published 2020 Sep 23.
17. Kumar R, Mooventhan A, Manjunath NK. Immediate effect of needling at CV-12 (Zhongwan) acupuncture point on blood glucose level in patients with type 2 diabetes mellitus: A pilot randomized Placebo-Controlled trial. J Acupunct Meridian Stud. 2017;10(4):240–4.
18. Li Y, Xie K, Zeng X, et al. Effect of Zuo's warming Yang acupuncture therapy combined with lifestyle interventions on prediabetes: A randomized controlled trial. Complement Ther Med. 2023;78:102985.
19. Liu R, He M, Zhao X, et al. Effects of stimulating single acupoint and combination acupoints on diabetic gastroparesis: A randomised controlled trial study. J Tradit Complement Med. 2024;14(4):446–55. Published 2024 Jan 23.
20. Wang Y, Xu GN, Wan RH, et al. Acupuncture in treating obesity combined with type 2 diabetes mellitus: A systematic review and meta-analysis of randomized controlled clinical trials. Complement Ther Clin Pract. 2022;49:101658.
21. Cao B, Li R, Tian H, et al. Effect on glycemia in rats with type 2 diabetes induced by streptozotocin: low-frequency electro-pulse needling stimulated Weiwanxiashu (EX-B 3) and Zusanli (ST 36). J Tradit Chin Med. 2016;36(6):768–78.
22. Huang XY, Zhang L, Sun J, et al. Acupuncture alters expression of insulin signaling related molecules and improves insulin resistance in OLETF rats. Evid Based Complement Alternat Med. 2016;2016:9651592.
23. Nakamura H, Ishigami T, Kawase Y, et al. Effects of acupuncture stimulation on blood glucose concentration in the Otsuka Long-Evans Tokushima fatty (OLETF) rat, an animal model for type-2 diabetes mellitus. Med Sci Monit Basic Res. 2014;20:70–5. Published 2014 May 19.
24. Xihui Q, Jianli P, Guan X, et al. Bo's abdominal acupuncture improves disordered metabolism in obese type 2 diabetic rats through regulating fibroblast growth factor 21 and its related adipokines. J Tradit Chin Med. 2023;43(6):1200–8.
25. Huang X, Huang K, Li Z, et al. EA improves cognitive deficits and insulin resistance in an OLETF rat model of AI/D-gal induced aging model via the PI3K/Akt signaling pathway. Brain Res. 2020;1740:146834.
26. Han X, Chen X, Wang X, et al. EA at ST36 improve the gastric motility by affecting neurotransmitters in the enteric nervous system in type 2 diabetic rats. Evid Based Complement Alternat Med. 2021;2021:6666323.
27. Jia X, Li M, Zhang W, et al. Adjusting internal organs and dredging Channelon EA glycolipid metabolism disorders in NAFLD mice by mediating the AMPK/ACC signaling pathway. Diabetol Metab Syndr. 2024;16(1):173.
28. Longo S, Rizza S, Federici M. Microbiota-gut-brain axis: relationships among the vagus nerve, gut microbiota, obesity, and diabetes. Acta Diabetol. 2023;60(8):1007–17.
29. Baars DP, Fondevila MF, Meijnikman AS, et al. The central role of the gut microbiota in the pathophysiology and management of type 2 diabetes. Cell Host Microbe. 2024;32(8):1280–300.
30. Richards P, Thornberry NA, Pinto S. The gut-brain axis: identifying new therapeutic approaches for type 2 diabetes, obesity, and related disorders. Mol Metab. 2021;46:101175.

31. Ma Q, Li Y, Li P, et al. Research progress in the relationship between type 2 diabetes mellitus and intestinal flora. Biomed Pharmacother. 2019;117:109138.
32. Umirah F, Neoh CF, Ramasamy K, et al. Differential gut microbiota composition between type 2 diabetes mellitus patients and healthy controls: A systematic review. Diabetes Res Clin Pract. 2021;173:108689.
33. Wang TY, Zhang XQ, Chen AL, et al. A comparative study of microbial community and functions of type 2 diabetes mellitus patients with obesity and healthy people. Appl Microbiol Biotechnol. 2020;104(16):7143–53.
34. Yang G, Wei J, Liu P, et al. Role of the gut microbiota in type 2 diabetes and related diseases. Metabolism. 2021;117:154712.
35. Wang Y, Dilidaxi D, Wu Y, et al. Composite probiotics alleviate type 2 diabetes by regulating intestinal microbiota and inducing GLP-1 secretion in Db/db mice. Biomed Pharmacother. 2020;125:109914.
36. Fukui H. Increased intestinal permeability and decreased barrier function: does it really influence the risk of inflammation?? Inflamm Intest Dis. 2016;1(3):135–45.
37. Ding S, Lund PK. Role of intestinal inflammation as an early event in obesity and insulin resistance. Curr Opin Clin Nutr Metab Care. 2011;14(4):328–33.
38. Zhou Y, Zhang D, Cheng H, et al. Repairing gut barrier by traditional Chinese medicine: roles of gut microbiota. Front Cell Infect Microbiol. 2024;14:1389925.
39. Zhang XY, Chen J, Yi K, et al. Phlorizin ameliorates obesity-associated endotoxemia and insulin resistance in high-fat diet-fed mice by targeting the gut microbiota and intestinal barrier integrity. Gut Microbes. 2020;12(1):1–18.
40. Pan Y, Bu T, Deng X, Jia J, Yuan G. Gut microbiota and type 2 diabetes mellitus: a focus on the gut-brain axis. Endocrine. 2024;84(1):1–15.
41. Price NL, Fernández-Tussy P, Varela L, et al. microRNA-33 controls hunger signaling in hypothalamic AgRP neurons. Nat Commun. 2024;15(1):2131.
42. Siemian JN, Arenivar MA, Sarsfield S, Aponte Y. Hypothalamic control of interoceptive hunger. Curr Biol. 2021;31(17):3797–e38095.
43. Li S, Liu M, Cao S, et al. The mechanism of the Gut-Brain axis in regulating food intake. Nutrients. 2023;15(17):3728.
44. Clarke GS, Page AJ, Eldeghaidy S. The gut-brain axis in appetite, satiety, food intake, and eating behavior: insights from animal models and human studies. Pharmacol Res Perspect. 2024;12(5):e70027.
45. Taheri R, Mokhtari Y, Yousefi AM, Bashash D. The PI3K/Akt signaling axis and type 2 diabetes mellitus (T2DM): from mechanistic insights into possible therapeutic targets. Cell Biol Int. 2024;48(8):1049–68.
46. Meng EX, Verne GN, Zhou Q. Macrophages and gut barrier function: guardians of Gastrointestinal health in Post-Inflammatory and Post-Infection responses. Int J Mol Sci. 2024;25(17):9422.
47. Li W, Du Q, Li X, et al. Eriodictyol inhibits proliferation, metastasis and induces apoptosis of glioma cells via PI3K/Akt/NF-κB signaling pathway. Front Pharmacol. 2020;11:114.
48. Taheri R, Mokhtari Y, Yousefi AM, et al. The PI3K/Akt signaling axis and type 2 diabetes mellitus (T2DM): from mechanistic insights into possible therapeutic targets. Cell Biol Int. 2024;48(8):1049–68.
49. Xie L, Chen T, Qi X, et al. Exopolysaccharides from Genistein-Stimulated monascus purpureus ameliorate Cyclophosphamide-Induced intestinal injury via PI3K/AKT-MAPKs/NF-κB pathways and regulation of gut microbiota. J Agric Food Chem. 2023;71(35):12986–3002.
50. Zhang H, Diao F. Nourishing Yin and moistening dryness formula inhibits colon cell apoptosis via activating the PI3K/AKT signaling pathway to ameliorate Yin-deficiency constipation in mice. J Funct Foods. 2023;110:105821.
51. Cao BY, Li R, Tian HH, et al. PI3K-GLUT4 signal pathway associated with effects of EX-B3 EA on hyperglycemia and insulin resistance of T2DM rats. Evid Based Complement Alternat Med. 2016;2016:7914387.
52. Pan T, Li X, Guo X, et al. EA improves insulin resistance in type 2 diabetes mice by regulating intestinal flora and bile acid. Diabetes Metab Syndr Obes. 2023;16:4025–42.
53. Wang H, Chen X, Chen C, et al. EA at lower He-Sea and Front-Mu acupoints ameliorates insulin resistance in type 2 diabetes mellitus by regulating the intestinal flora and gut barrier. Diabetes Metab Syndr Obes. 2022;15:2265–76.
54. Zhang L, Chen X, Wang H, et al. Adjusting internal organs and dredging channel EA ameliorates insulin resistance in type 2 diabetes mellitus by regulating the intestinal flora and inhibiting inflammation. Diabetes Metab Syndr Obes. 2021;14:2595–607.
55. Zhu Y, Tian J, Wei X, Jia S, Shu Q. EA alleviates obesity and insulin resistance via the GLP-1-VTADA reward circuit. Neuroendocrinology. 2024;114(3):263–78.
56. Duan H, Song S, Li R, et al. Strategy for treating MAFLD: electroacupuncture alleviates hepatic steatosis and fibrosis by enhancing AMPK mediated glycolipid metabolism and autophagy in T2DM rats. Diabetol Metab Syndr. 2024;16(1):218.
57. He Y, Yang K, Zhang L, et al. Electroacupuncture for weight loss by regulating microglial polarization in the arcuate nucleus of the hypothalamus. Life Sci. 2023;330:121981.
58. Xue NY, Ge DY, Dong RJ, et al. Effect of electroacupuncture on glial fibrillary acidic protein and nerve growth factor in the hippocampus of rats with hyperlipidemia and middle cerebral artery thrombus. Neural Regen Res. 2021;16(1):137–42.
59. Cao BY, Li R, Tian HH, et al. PI3K-GLUT4 signal pathway associated with effects of EX-B3 electroacupuncture on hyperglycemia and insulin resistance of T2DM rats. Evid Based Complement Alternat Med. 2016;2016:7914387.
60. Wang H, Liu WJ, Shen GM, et al. Neural mechanism of gastric motility regulation by electroacupuncture at RN12 and BL21: A paraventricular hypothalamic nucleus-dorsal vagal complex-vagus nerve-gastric channel pathway. World J Gastroenterol. 2015;21(48):13480–9.
61. Md Mokhtar AH, Malik IA, Abd Aziz NAA, Almabhouh FA, Durairajanayagam D, Singh HJ. LY294002, a PI3K pathway inhibitor, prevents leptin-induced adverse effects on spermatozoa in Sprague-Dawley rats. Andrologia. 2019;51(3):e13196.
62. Wu X, Pu L, Chen W, et al. LY294002 attenuates inflammatory response in endotoxin-induced uveitis by downregulating JAK3 and inactivating the PI3K/Akt signaling. Immunopharmacol Immunotoxicol. 2022;44(4):510–8.
63. Wang L, Yu CC, Li J, Tian Q, Du YJ. Mechanism of action of acupuncture in obesity: A perspective from the hypothalamus. Front Endocrinol (Lausanne). 2021;12:632324.
64. Sun X, Cui Y, Su Y, et al. Dietary fiber ameliorates Lipopolysaccharide-Induced intestinal barrier function damage in piglets by modulation of intestinal Microbiome. mSystems. 2021;6(2):e01374–20.
65. Li B, Wang Y, Yuan X, et al. 6-Shogaol from dried ginger protects against intestinal ischemia/reperfusion by inhibiting cell apoptosis via the BDNF/TrkB/PI3K/AKT pathway. Mol Nutr Food Res. 2023;67(13):e2200773.
66. Liu Z, Zhang Z, Chen X, Ma P, Peng Y, Li X. Citrate and hydroxycinnamate derivatives from Mume fructus protect LPS-injured intestinal epithelial cells by regulating the FAK/PI3K/AKT signaling pathway. J Ethnopharmacol. 2023;301:115834.
67. He S, Guo Y, Zhao J, Xu X, Wang N, Liu Q. Ferulic acid ameliorates Lipopolysaccharide-Induced barrier dysfunction via MicroRNA-200c-3p-Mediated activation of PI3K/AKT pathway in Caco-2 cells. Front Pharmacol. 2020;11:376.
68. Zou Z, Wang Z. Liraglutide attenuates intestinal ischemia/reperfusion injury via NF-κB and PI3K/Akt pathways in mice. Life Sci. 2022;309:121045.
69. Hao X, Ding N, Zhang Y, et al. Benign regulation of the gut microbiota: the possible mechanism through which the beneficial effects of manual acupuncture on cognitive ability and intestinal mucosal barrier function occur in APP/PS1 mice. Front Neurosci. 2022;16:960026.
70. Liu S, Huang Q, Huang Q, et al. The protective effects of EA on intestinal barrier lesions in IBS and UC model. Sci Rep. 2023;13(1):7276.
71. Kang X, Zhang H, Li X, et al. EA improving intestinal barrier function in rats with irritable bowel syndrome through regulating Aquaporins. Dig Dis Sci. 2024;69(4):1143–55.
72. Ma X, Wang Q, Yuan W, et al. EA alleviates neuroinflammation and motor dysfunction by regulating intestinal barrier function in a mouse model of Parkinson disease. J Neuropathol Exp Neurol. 2021;80(9):844–55.
73. Guo L, Hu H, Jiang N, et al. EA blocked motor dysfunction and gut barrier damage by modulating intestinal NLRP3 inflammasome in MPTP-induced Parkinson's disease mice. Heliyon. 2024;10(9):e30819.
74. Xu H, Wen Q, Hu H, et al. EA at ST36 modulates the intestinal microecology and May help repair the intestinal barrier in the rat model of severe acute pancreatitis. Microb Biotechnol. 2024;17(2):e14401.
75. Li F, Zhang G, Liang J, et al. Protection of intestinal barrier in uremic mice by EA via regulating the cannabinoid 1 receptor of the intestinal glial cells. J Biomed Nanotechnol. 2021;17(11):2210–8.
76. Tian J, Bai B, Gao Z, et al. Alleviation effects of GQD, a traditional Chinese medicine formula, on diabetes rats linked to modulation of the gut Microbiome. Front Cell Infect Microbiol. 2021;11:740236.
77. Cao Z, Wang X, Liu H, Yang Z, Zeng Z. Gut microbiota mediate the alleviation effect of Xiehuo-Guzheng granules on B cell dedifferentiation in type 2 diabetes mellitus. Phytomedicine Published Online Oct. 2024;16. https://doi.org/10.1016/j.phymed.2024.156151.
78. Yang F, Li J, Wei L, et al. The characteristics of intestinal microbiota in patients with type 2 diabetes and the correlation with the percentage of T-helper cells. Front Microbiol. 2024;15:1443743.

79. Ding L, Teng R, Zhu Y, et al. EA treatment ameliorates metabolic disorders in obese ZDF rats by regulating liver energy metabolism and gut microbiota. Front Endocrinol (Lausanne). 2023;14:1207574.
80. Wang H, Wang Q, Liang C, et al. Acupuncture regulating gut microbiota in abdominal obese rats induced by High-Fat diet. Evid Based Complement Alternat Med. 2019;2019:4958294.
81. DeSantis TZ Jr, Hugenholtz P, Keller K et al. NAST: a multiple sequence alignment server for comparative analysis of 16S rRNA genes. Nucleic Acids Res. 2006;34(Web Server issue):W394–9.
82. Zhu Y, Chen B, Zhang X, et al. Exploration of the muribaculaceae family in the gut microbiota: diversity, metabolism, and function. Nutrients. 2024;16(16):2660.
83. Zhao Y, Yang H, Wu P, et al. Akkermansia muciniphila: A promising probiotic against inflammation and metabolic disorders. Virulence. 2024;15(1):2375555.

Publisher's note